Korean J. Chem. Eng., 34(8), 2342-2353 (2017)
DOI: 10.1007/s11814-017-0127-9

pISSN: 0256-1115
eISSN: 1975-7220

Decolorization of Direct Blue 71 solutions using tannic acid/polysulfone thin film nanofiltration composite membrane; preparation, optimization and characterization of anti-fouling

Nader Yousefi*, Ramin Nabizadeh*, Simin Nasseri*,, Mehdi Khoobi***,****, Shahrokh Nazmara*, and Amir Hossein Mahvi*,**,*****,******,†**

*Department of Environmental Health Engineering, School of Public Health, Tehran University of Medical Sciences, Tehran, Iran
**Center for Water Quality Research (CWQR), Institute for Environmental Research (IER), Tehran University of Medical Sciences (TUMS), Tehran, Iran
***Medical Biomaterials Research Center, Tehran University of Medical Sciences, Tehran, Iran
****Department of Medicinal Chemistry, Faculty of Pharmacy and Pharmaceutical Sciences Research Center, Tehran University of Medical Sciences, Tehran 14176, Iran
*****Center for Solid Waste Research (CSWR), Institute for Environmental Research (IER), Tehran University of Medical Sciences (TUMS), Tehran, Iran
******National Institute of Health Research, Tehran University of Medical Sciences, Tehran, Iran
(*Received 8 March 2017 • accepted 6 May 2017*)

Abstract−The objective of this research was to use tannic acid (TA) as polyphenol monomer and trimesoyl chloride (TMC) to synthesize the nano-composite membranes and its application for dye removal from water. The combined effects of factors were studied by response surface methodology (RSM). Synthesized membrane was characterized by field emission scanning electron microscopy (FESEM), atomic force microscopy (AFM), attenuated total reflection Fourier transform infrared spectroscopy (ATR-FTIR) and water contact angle measurement. The results showed that monomer concentrations and post treatment (time and temperature) had a significant effect on the membrane synthesis. The predicted optimum operational conditions were initial direct blue 71 concentration of 30.31 mg/L; time of 16.96 min, applied pressure of 1.16 bar. Fouling mechanism was pore sealing (n=1.96). The excellent antifouling properties and resistance ability to organic and chemical reagents of the prepared composite nanofiltration membranes caused to suggest this membrane for water treatment.

Keywords: Thin Film Layer, Tannic Acid, Decolorization, Interfacial Polymerization, Response Surface Methodology

INTRODUCTION

Synthetic dyes have been widely used in industries such as textile, tanning, printing, drug and food processing, paper and agricultural technologies, ground water tracing and hair coloring [1-3]. Synthetic dyes have a varied structure. The azo, sulfur, triphenylmethyl, phthalocyanine, anthraquinone and indigoid are the most chemical classes of dyes. However, the azo derivatives are the majority of synthetic dyes employed in the industry. More than 100000 dyes are commercially recognized and the amount of dyes produced in the world is estimated about 10000 tons per year [4-6]. And it is estimated that about 1-2% in the production phase (about 40-65 L of textile effluent per kg of produced cloth [7,8] and 1-10% in the use phase can be discharged to the environment. Also, textile wastewater contains high suspended solids, chemical oxygen demand, biological oxygen demand, heat and chemicals such as salts as well as high color [9,10]. The synthetic dyes have a complex aromatic structure that makes them increasingly resistant to biodegradation and being stable [11-13]. Thus, dye wastewater is potentially carcinogenic and toxic for the environment [2,14,15]. Therefore, synthetic dyes can have adverse effects on the environment as well as health. The environmental concern related to synthetic dyes is due to their recalcitrant nature as well as their high visibility [1,7,16]. Several technologies have been employed for synthetic dye removal from colored waters and wastewaters that involve biological or enzymatic processes, adsorption, photocatalysis, oxidation process, membrane filtration, precipitation and ion exchange [9,11,17]. High cost, low efficiency and complexity of the operation and maintenance are the disadvantage of these technologies [2].

Nanofiltration, which has been widely used in water and wastewater treatment, can separate the multivalent ions and small molecules [18-20]. The aim of the ultrathin layer of TFC membrane is to reject salts while penetrating water and reaching to minimum energy consumption [21-24]. Interfacial polymerization (IP) is a process which starts with imbuing a porous support membrane with an aqueous solution (polyfunctional amine) and then soaking with an organic solution (polyfunctional acyl chloride) dissolved in immiscible solvents to induce interfacial polymerization. IP is able

†To whom correspondence should be addressed.
E-mail: ahmahvi@yahoo.com

to generate ultrathin, polymeric network forms and solvent resistant and cross-linked layer (100 nm) [21,25,26]. The interfacial polymerization reaction depends on the support membrane characteristics [21]. Therefore, monomers and support membrane can be dependently optimized for TFC membrane performance due to properties and structure of the prepared membrane, which highly depends on properties and structure of support membrane [25,27]. Surface roughness obviously affects the membrane fouling and scaling. Membrane with smoother surfaces has less fouling and scaling than rougher membranes. Therefore, modifying the membrane surface by IP could reduce the fouling and scaling inclination [28, 29]. The prepared membrane through IP has high permeability, water flux and considerable salt rejection [30].

Tannic acid is a polyphenolic compound able to establish complex chemical structures. The chemical formula of tannic acid is $C_{76}H_{52}O_{46}$ which is a commercial form of tannins. Due to the high capacity of these compounds, these products are used at industrial and experimental levels. Tannic acid as a polyphenol can react with acyl chloride at interfacial zone of aqueous and organic phase and generate a cross-linking thin film on the ultrafiltration porous support.

IP reactions and then thin film formation have been required to be optimized to attain high membrane performance for each monomer [25]. Response surface method (RSM) is a statistical method for optimizing the physical, chemical and biological experimental processes [31,32]. In this study, RSM was employed to design the membrane synthesis by interfacial polymerization and operational conditions. Therefore, the main goal of this research was to investigate membrane synthesis by interfacial polymerization methods and application of synthesized nanocomposite membrane for dye removal from water.

MATERIAL AND METHODS

1. Materials

Piperazine (PIP), N-N Dimethylformamide (DMF), Tannic acid (TA), Trimesoyl chloride (TMC, or 1,3,5-benzenetricarbonyltrichloride), HCl and NaOH were obtained from Sigma-Aldrich USA in analytical grade. Humic acid (HA), Bovine serum albumin (BSA), n-hexane, sodium hypochlorite, NaOH, and Na_2CO_3 were purchased from Merck (Germany). Direct blue 71 (DB71), reactive blue 19 (RB19) and methylene blue (MB) were obtained from CIBA (Switzerland). All chemicals used in this study were analytical grade. The deionized (DI) water was used for the sample preparation and pure water flux measurements.

2. Analytical Methods

UV-Vis spectrophotometer (Perkin Elmer, lambda 25, USA) was used to measure the DB71 dye concentration at maximum adsorption wavelength. Also, BSA and HA concentration were measured through UV-Vis spectrophotometer at wavelengths of 278 and 254, respectively. To determine the size of pores and morphology of membrane, photos of membrane were taken through field emission scanning electron microscope (Mira 3 Tescan, Czech Republic) at the accelerating voltage of 15 KV. Attenuated total reflectance Fourier transform infrared spectroscopy (ATR-FTIR) spectrometer (ensor 27, Bruker Inc., Germany) was used to provided Infra-red (IR) spectra, and top surface morphology and roughness analysis was determined by atomic force microscopy (AFM) (Thermo microscopes Auto probe CP Research, Veeco Instruments, Sunnyvale, CA, USA). The contact angle and zeta potential was measured using a water contact angle measurement (OCA 15 Plus, Dataphsycs, Germany) and streaming potential method (Electro kinetic Analyzer (EKA, Anton Paar GmbH, Austria)), respectively.

3. Preparation of Composite Nanofiltration Membranes

Interfacial polymerization (IP) method was used for providing the composite nanofiltration membranes. Polysulfone (PSf) ultrafiltration membranes were applied as a support substrate membrane to synthesize the composite membrane. The molecular weight cut off (MWCO) of support membrane was about 50000 and pure water flux was 130 L/m^2·h at 1 bar pressure. Aqueous phase solutions were provided through TEOA (6%, w/v), SDS (0.3%, w/v) and different concentrations of tannic acid (0 to 0.3 wt%) in deionized water. pH of aqueous solution was redacted using the mixture of NaOH and Na_2CO_3 which NaOH to Na_2CO_3 ratio was 1 : 2. While the organic phase solution was obtained from dissolving different concentrations of TMC (0 to 0.3 wt%) in n-hexane solvent. Before using the PSf as a porous membrane, membrane was hydrophilized with acetone and then the chromic acid solution for 30 min at 65 °C before the IP reaction. Finally, membrane was completely washed and soaked in water for 24 h. According to the IP reaction, the PSf membranes were first saturated in organic solution for about 30 min. The PSf saturated with TMC was secondly immersed into the aqueous solution (TA solution) for 35 min to release the tannic acid into the porous support. Then, the excess solution of TA solution was removed from the surface of membrane with filter papers. The saturated membrane was doubly soaked into the TMC solution (organic phase) to guarantee that polymerization reaction has been taken place. After separating excess TMC with filter paper, the nanocomposite membrane was dried in an oven for an exact time (10-30) and temperature (20-80 °C) for further polymerization and evaporating n-hexane (post treatment). Finally, the nanocomposite membrane was washed and stored in distilled water for investigating the membrane performance and characteristics.

4. Experimental Design

4-1. Experimental Design for Preparation of Composite Nanofiltration Membranes

CCD method was employed to study preparation of composite nanofiltration membranes for DB 71 removal. RSM was applied to determine the interaction effects of TA concentration, TMC concentration (X2), temperature (X3), time (X4) on the DB71 removal and flux (Y1 and Y2). To achieve the goal of this stage, a full factor design with four above-mentioned controllable variables was done. The coded values of independent variables used for experimental design are presented in Table 1.

Totally, 44 experiments were conducted using 2k (k was the number of variables) and that included 21 replicates in the center point, according to orthogonal CCD in two cube and star blocks. The coded values were coded based on following Equation:

$$X_i = \frac{X_0 - X_1}{\Delta X}$$

where X_i (dimensionless) is a coded value for the ith independent variable, X_0 is the uncoded value for the test variable at the center

Table 1. Experimental ranges and levels of the independent test variables

Parameters	Coded value	$-\alpha$	−1	0	+1	$+\alpha$
Tannic acid (mg/L)	X1	0	0.075	0.15	0.225	0.3
TMC (mg/L)	X2	0	0.075	0.15	0.225	0.3
Temperature (°C)	X3	20	35	50	65	80
Time (min)	X4	10	15	20	25	30

point and X_2 is the center point value of X_i, and ΔX is the step change value. A quadratic (second order) model was used to estimate the interaction between DB71 removal and flux as a response (Y) and four independent variables that are shown in the following equation:

$$Y = b_0 + \sum_{i=1}^{k} b_i X_i + \sum_{i=1}^{k} b_{ii} X_i^2 + \sum_{i=1}^{k-1} \sum_{j=2}^{k} b_{ij} X_i X_j + C$$

where Y shows the dependent variable, b_0 represents a constant value, b_i is regression coefficient for linear order and b_{ii}, and b_{ij} are the regression coefficient for second-order and interactive effects, respectively, X_i and X_j refer to the independent variables, and C represents the error of prediction. R software for windows (Version 3.2.2) was used for calculate the coefficients related to the CCD and statistical analysis such as ANOVA, t-test and F-test.

4-2. Experimental Design for Optimization of the Operational Parameters for DB71 Removal

Central composite design (CCD) was also used to determine the DB71 removal. The RSM was utilized to assess the composed effects of dye concentration (X1), time (X2) and pressure applied (X3) on the separation process. Note that pressure applied was considered in three levels in addition to two other parameters. The experimental levels of independent test variables, which were designed through CCD method, are summed up in Table 2. The removal efficiency of DB71 (Y) was considered as a response. This design was done with two blocks, and a total of 63 experiments were carried out, consisting of 42 center points, 2^3=8 design point, and 2×3=6 axial points. The experimental ranges and levels of the independent test variables are given in Table 2.

Table 2. Experimental ranges and levels of the independent test variables for DB71 removal

Parameters	Code	$-\alpha$	−1	0	+1	$+\alpha$
DB71 (mg/L)	X1	25	38.53	62.5	85.46	100
Time (min)	X2	10	16.36	35	53.63	60
Pressure (bar)	X3	1	2	3	4	5

5. Membrane Characteristics

To determination the membrane porosity and pore size of the prepared membrane, gravimetry method was employed. The prepared membranes were separated into 1×1 cm pieces and dried in an oven at 50 °C for 24 h. The dried membrane were weighted and the pieces of the membranes were soaked in deionized water for 24 h at room temperature. Then, the water droplets were removed from the surface of the membranes using a filter paper filter and the membrane was weighted again. Finally, the porosity of the membrane (ε) was calculated by using the following equation [33]:

$$\varepsilon = \frac{\frac{w_1 - w_2}{\rho_w}}{\frac{w_1 + w_2}{\rho_w} + \frac{w_2}{\rho_m}} \times 100\%$$

where, ε is porosity (%), w_1 and w_2 refer to wet and dry weights of

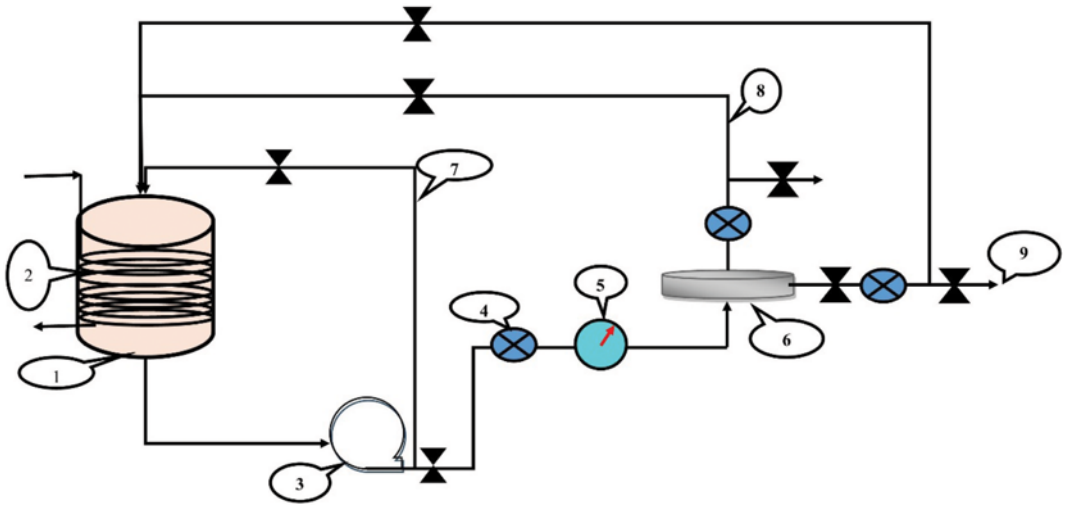

Fig. 1. Schematic and membrane filtration system used in this study.

1. Feed tank
2. Cooling circuit
3. Low pressure pump
4. Gauge
5. Flow meter
6. Membrane Module
7. Circulate line
8. Concentrate ling
9. Permeate line

membrane (g), ρ_m represents the density of the polymer (at 25 °C for PSf=1.24 g/mL), and ρ_w presents the density of distilled water (0.998 g/mL at 25 °C).

The average radius of the membrane pore size was computed by Guerout-Elford-Ferry equation:

$$r_m = \sqrt{\frac{(2.9-1.75\varepsilon)\times 8\eta l Q}{\varepsilon \times A \times \Delta P}}$$

where, r_m represents the average of pore radius (m), ε refers to porosity, η and l present water viscosity (8.9×10^{-4} Pa·s) and the thickness of the membrane (m), Q, A and ΔP are the permeate water flow (m^3/s), the effective area of the membrane used (m^2) and the operational pressure (Pa), respectively [33]. Membrane porosity and pore size were determined through BET analysis.

6. Permeation and DB71 Rejection Experiments

To evaluate the performance of composite membranes on the DB71 separation, a stainless steel dead-end filtration system with a feed volume of 2 L and an effective membrane area of 9.6 cm^2 was used. Details of this setup are illustrated in Fig. 1.

To measure the pure water flux and DB71 rejection, cross flow membrane module was used at 2 bar operation pressure. The water flux was computed with following equation:

$$J_w = \frac{V}{At}$$

where, J_w represents water flux ($L/m^2\cdot h$), V refers to the volume of the permeated pure water (L), A and t are the effective area of the membrane (m^2) and sampling time (h), respectively. Also, the DB71 removal efficiency was calculated as:

$$R(\%) = 1 - \frac{C_p}{C_f}\times 100$$

where, R represents the removal efficiency (%), C_p and C_f refer to DB71 concentration (mg/L) in the permeate and feed tank, respectively.

7. Performance of Prepared Membrane at Optimum Condition

To evaluate the performance of prepared composite membrane at optimum condition, methylene blue, Reactive Blue 19 and DB71 in different concentration (25-100 mg/L) were selected as the pollutants. In this stage, all parameters (including membrane synthesis and operational factors) were chosen according to the optimum conditions.

8. Antifouling Estimation of Composite Nanofiltration Membranes

BSA, HA and sodium sulfate (Na_2SO_4) were used to estimate the antifouling properties of prepared membrane. The antifouling experiments were done for 25 h. The concentration of BSA, HA and Na_2SO_4 in the feed tank was 100 mg/L, 100 mg/L and 500 mg/L, respectively.

The flux decay ratio (FDR) was calculated by the following equation:

$$FDR = \left[\frac{J_0 - J_t}{J_0}\right]\times 100$$

where J_0 and J_t represent the flux at the initial time and at time t, respectively. Then, the fouled membrane was washed with distilled water, NaOH (1 N), HCl (1 N) and ultrasound (130 KHz) to evaluate the recovery ratio. The flux recovery ratio (FRR) is calculated by below equation:

$$FRR(\%) = \left[\frac{J_t}{J_0}\right]\times 100$$

9. Fouling Study of Composite Nanofiltration Membrane

The Hermia empirical model was used to evaluate the fouling mechanisms. To achieve this goal, the system was run as a dead-end state at constant pressure (1 bar). Permeate volume was determined at certain intervals and then the mechanism fouling was ascertained.

RESULT AND DISCUSSION

1. Membrane Characteristics

FTIR-ATR was used to evaluate the incorporation of hydrophilic polymers on the PSf porous support membrane. In the interfacial zone between aqueous solution (contain TA) and organic solution (contain TMC), TA as a plant polyphenol could react with acyl chloride in order to make a crosslink thin film on the porous support membrane. As illustrated in Fig. 2, the FTIR spectrum of TA presents some peaks at 1,748, 1,628, 1,443 and 1,309 cm^{-1}. Because the signal bands of carbonyl groups (C=O) and etheric bands (C-O) emerge at 1,710-1,780 cm^{-1} and 1,100-1,300 cm^{-1}, respectively, it shows that TA contains aromatic esters. According to the FTIR-ATR results of the composite membranes, the signal bonds of 1,765 cm^{-1} and 1,244 cm^{-1} belong to C=O and C-O (etheric group) bands, respectively. In addition, increasing in concentration of TA and TMC can be lead to intensification of signal bond of ester groups. As appears in Fig. 2, band signals of H-O-H at 1,748 and 1,628 cm^{-1} in tannic acid and nanocomposite spectra are observable.

The impact of interfacial polymerization by TA and TMC on the final membrane surface structure and formation of ultra-thin skin layer can be distinguished by FESEM image. Surface SEM images and AFM for the support membrane and nanocomposite membranes are presented in Fig. 3. According to the images of

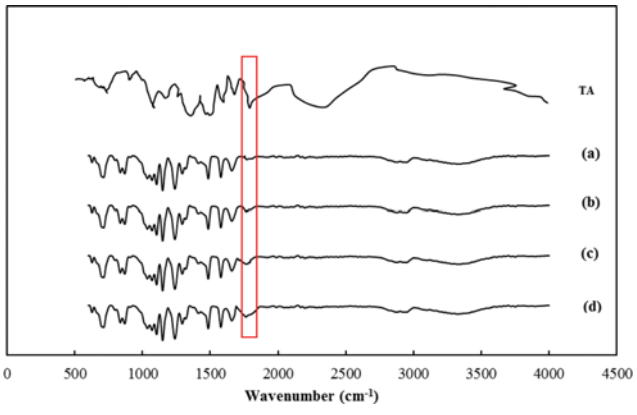

Fig. 2. ATR-FTIR of tannic acid and synthesized membrane TA: Tannic Acid, (a) PSF support (b) AT: 0.1 TMC: 0.3 (c) AT: 0.3 TMC: 0.1 (d) AT: 0.3 TMC: 0.3.

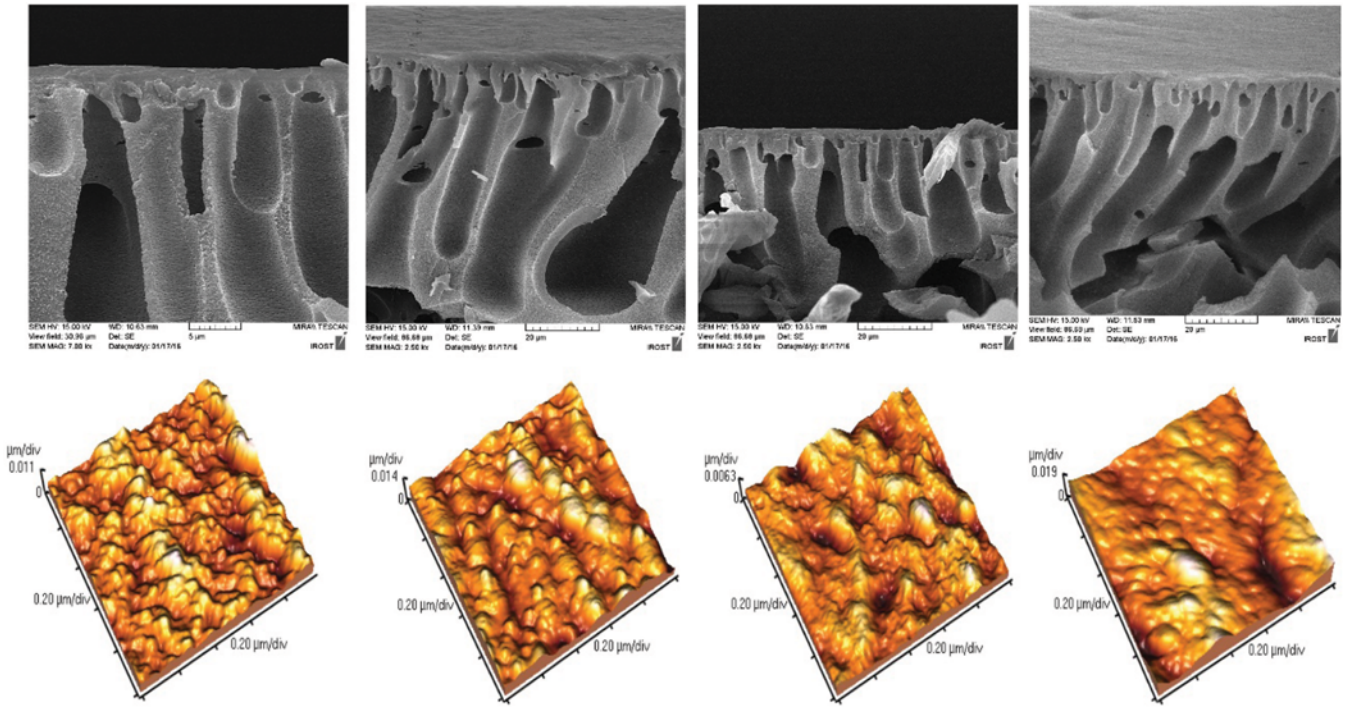

Fig. 3. Cross-section FESEM micrographs and AFM images of synthesized nanocomposite membranes; (a) AT: 0.1 TMC: 0.3 (b) AT: 0.3 TMC: 0.1 (c) AT: 0.3 TMC: 0.3.

Table 3. Mean pore radius, water contact angle, porosity and pure water flux parameters of the prepared membranes

Membrane	TA (mg/L)	TMC (mg/L)	Mean pore radius (nm)	Contact angle (degree)	Porosity (%)	Flux (L/m^2·h) at 1 bar	Surface zeta potential
PSF	-	-	22.3±0.63	59.3±2.1	73.1±2.53	130±4.52	−12.1±1.3
1	0.1	0.3	19.2±0.41	62.2±2.25	61.3±1.42	73.9±2.43	−15.9±0.9
2	0.3	0.1	11.6±0.59	65.1±1.6	48.5±2.11	52.5±3.12	−18.8±2.5
3	0.3	0.3	4.46±0.73	67.8±1.3	38.23±2.23	41.3±2.45	−19.9±3.2

SEM, a thin tedium film of the polymeric layer was generated on the ultrafiltration support membrane. Before the preparation of nanocomposite membrane, the ultrafiltration support membrane surfaces exhibit a peaks-and-valley morphology structure. So the surface of the composite membrane demonstrates a dense smooth structure. Denser and smoother structure can result in decreasing the permeability. According to the AFM images, increasing in TA and TMC concentration caused to decrease the membrane surfaces roughness. This phenomenon can confirm that the depth of TA and TMC in the water interfacial zone is limited.

Table 3 shows the characteristics of nanocomposite membrane. According to this table, the porosity of the prepared nanocomposite membrane decreases with increasing in the concentration of monomers (tannic acid in aqueous phase and TMC in organic phase). In this phenomenon, the pores of composite membrane are obstructed in the high concentrations of monomers, which leads to decrease in permeability [34]. These results were found in the similar works [35]. Also, contact angle increases with the increasing in the TA and TMC concentration ratio. On the other hand, the contact angle is slightly changed with increasing in the TMC concentration, which indicates TMC concentration had a little effect on hydrophilicity of the surface. Decreasing in intermediate energy (interface energy) with water is carried out due to increasing the hydrophilic groups on the membrane surface. As a matter of fact, decreasing in the contact angle may be happening with increasing the hydrophilic groups on the membrane [36].

According to the results, the zeta potential of the membrane is shown in Table 3. All values of zeta potential for all membrane are negative. Increasing in the monomer concentration can lead to increase in negative charge and zeta potential. Accordingly, net PSF membrane had the lowest zeta potential and membrane with the maximum monomer concentrations (no. 3) had the lowest value. Flux, rejection rate and anti-fouling properties of membranes depend on the zeta potential value [37]. Functional groups on the membrane determine the surface charge on the membrane. Presence of carboxylic and hydroxylic functional groups on the membrane can induce the negative charges on the nanocomposite membrane [38]. Indeed, Donnan repulsion or adsorption of pollutants by the membrane are the main removal mechanism and functional groups determine the repulsion and/or adsorption mechanism. In this case,

Table 4. Observed and predicted values of DB71 removal for the quadratic model

Run no.	X1	X2	X3	X4	R (%)	Predicted (%)	Run no.	X1	X2	X3	X4	R (%)	Predicted (%)
1	0.225	0.075	35	15	60.2	55.9	23	0.075	0.225	35	25	75.2	86.5
2	0.15	0.15	50	20	79.3	75.01	24	0.225	0.075	35	25	74.8	80.4
3	0.15	0.15	50	20	76.2	76.01	25	0.15	0.15	50	20	71.3	71.25
4	0.075	0.075	65	25	83.5	80.47	26	0.15	0.15	50	20	73.8	70.6
5	0.075	0.075	65	15	55.8	55.9	27	0.225	0.225	65	15	74.6	66.5
6	0.15	0.15	50	20	69.6	69.01	28	0.15	0.15	50	20	75.7	69.03
7	0.075	0.075	35	25	81.9	78.07	29	0.15	0.15	50	20	67.6	70.2
8	0.225	0.075	65	15	64.9	58.3	30	0.15	0.15	50	20	47.1	74.5
9	0.225	0.225	35	25	93.2	92.9	31	0.15	0	50	20	76.5	67.5
10	0.15	0.15	50	20	78.6	77.01	32	0.15	0.15	50	10	91.9	39.8
11	0.075	0.225	65	15	65.4	58.45	33	0.15	0.15	50	20	75.3	74.9
12	0.15	0.15	50	20	75.6	71.01	34	0.15	0.15	50	30	71.3	88.8
13	0.225	0.075	65	25	91.6	89.83	35	0.15	0.15	50	20	72.9	71.04
14	0.15	0.15	50	20	77.8	73.01	36	0	0.15	50	20	74.6	66.65
15	0.15	0.15	50	20	71.6	69.01	37	0.15	0.15	50	20	84.9	69.01
16	0.075	0.225	65	25	92.3	89.9	38	0.15	0.15	50	20	74.3	69.01
17	0.075	0.075	35	15	57.4	53.57	39	0.15	0.15	80	20	88.9	80.8
18	0.225	0.225	35	15	70.4	68.4	40	0.15	0.15	20	20	74.3	72.03
19	0.075	0.225	35	15	68.3	56.06	41	0.15	0.3	50	20	81.5	82.5
20	0.225	0.225	65	25	94.9	92.3	42	0.15	0.15	50	20	71.8	70.2
21	0.15	0.15	50	20	74.2	70.1	43	0.3	0.15	50	20	75.2	81.3
22	0.15	0.15	50	20	75.4	72.0	44	0.15	0.15	50	20	74.8	69.01

hydroxyl and carboxylic groups on the membrane can increase the repulsion mechanism on the membrane. Functional groups in the tannic acid can move on the membrane surface and create a negatively charged surface during the interfacial polymerization. In addition, negative charge of DB71 and negative charge of the nanocomposite membrane can augment the Donnan repulsion and then increase in the rejection rate of DB71. Generally, ion capacity, membrane and ion charge and ionic strength determine the charge repulsion of the target ions in the aqueous solution [39]. Therefore, it seems that Donnan repulsion was the main mechanism of DB71 removal from aqueous solution through the nanocomposite. Thus, antifouling properties of the nanocomposite membrane improve with decreasing the zeta potential for DB71 removal. As a matter of fact, the presence of hydroxyl groups on the membrane surface results in the excellent antifouling properties of nanocomposite membranes and can prevent contact and firmly adsorbing the foulant ions and molecules to the membrane surface. Moreover, previous studies have suggested that strong bonds of membrane with water also could effectively increase the rejection of molecules [40].

2. Preparation of Composite Nanofiltration Membranes

Porous support layer and dense skin layer are the main structure of the nanocomposite membrane. The determining factors on the nanocomposite performance are the preparation conditions and the chemistry of ultra-thin selective layer. Thus, evaluating the main factors on the membrane preparation is required. Therefore, in this step, effective factors on the membrane preparation such as the monomer concentration in immiscible solvents as well as post treatment factors (temperature and reaction time) were studied to achieve the optimal conditions for membrane synthesis. According to central composite design (CCD), experimental and predicted values of water flux conducted on the prepared nanocomposite membranes using quadratic model are represented in Tables 4. Analysis of variance (ANOVA) for the membrane preparation and regression analysis for the quadratic model are shown in Table 5. As seen, the predicted data had a good agreement with the experimental data (R^2>0.96), which indicates the quadratic model was in line with forecasting the preparation conditions for composite membranes (Table 5). According to the results, the effect of all parameters was significant for membrane preparation, but the effect of X1 and X2 (TA and TMC concentration) and X4 (time) were significantly higher than the X3 (temperature).

As seen in Table 4, the water flux decreased with increasing monomer concentration. It could result in increasing in the DB71 rejection. Decreasing in the water flux at the initial time was slow; then at high concentration of monomers, the water flux sharply decreased with more enhancement of monomer concentrations. It could be due to further reaction between TA and TMC in the interfacial zone. The results of monomer concentrations are clear that triacyl chloride functional groups of TMC reacts with the support ultrafiltration membrane, and the phenolic functional groups of TA also chemically make a cross-link with TMC. Further, cross-linking reaction between TA in aqueous phase and TMC in organic phase resulted in decreasing pore densities of the thin films prepared and subsequently water flux. In addition, the reaction time had a significant effect on the thin layer prepared on the support membrane (Fig. 4). As seen in the results, the water flux decreased with increasing in reaction time from 10 to 30 min. It could be due to reaction time, as a post treatment can diminish the degree

Table 5. Analysis of variance (ANOVA) and regression for the quadratic model in preparation of membrane

Analysis of variance (ANOVA)					
Model formula in RSM (X1, X2, X3, X4)	DF	Sum of squares	Mean squares	F-value	Probability (P)
FO	4	4264.5	1066.14	192.5047	<0.0002
TWI	6	41.2	6.87	1.2413	0.00314
PQ	4	154.3	38.58	6.9655	0.00046
Residuals	29	160.6	5.54	-	-
Lack of fit	10	58.4	5.84	1.0865	0.418
Pure error	19	102.2	5.38	-	-
Regression analysis for the quadratic model					
Parameter		Coefficient estimate	Std. error	t Value	Pr(>|t|)
(Intercept)		74.89	0.52622	142.315	2.2×10^{-16}
X_1		4.725	0.96075	4.918	3.19×10^{-5}
X_2		9.05833	0.96075	9.4284	2.47×10^{-10}
X_3		2.39167	0.96075	2.4894	0.018780
X_4		24.50833	0.96075	25.5096	2.20×10^{-16}
$X_1{*}X_2$		−3.77500	2.35335	−1.6041	0.095129
$X_1{*}X_3$		3.77500	2.35335	1.6041	0.095219
X_2^2		4.06417	1.60764	2.528	0.017173
Multiple R^2=0.965; Adjusted R^2=0.948; Predicted R^2: 0.947, Lack of fit: 0.322					

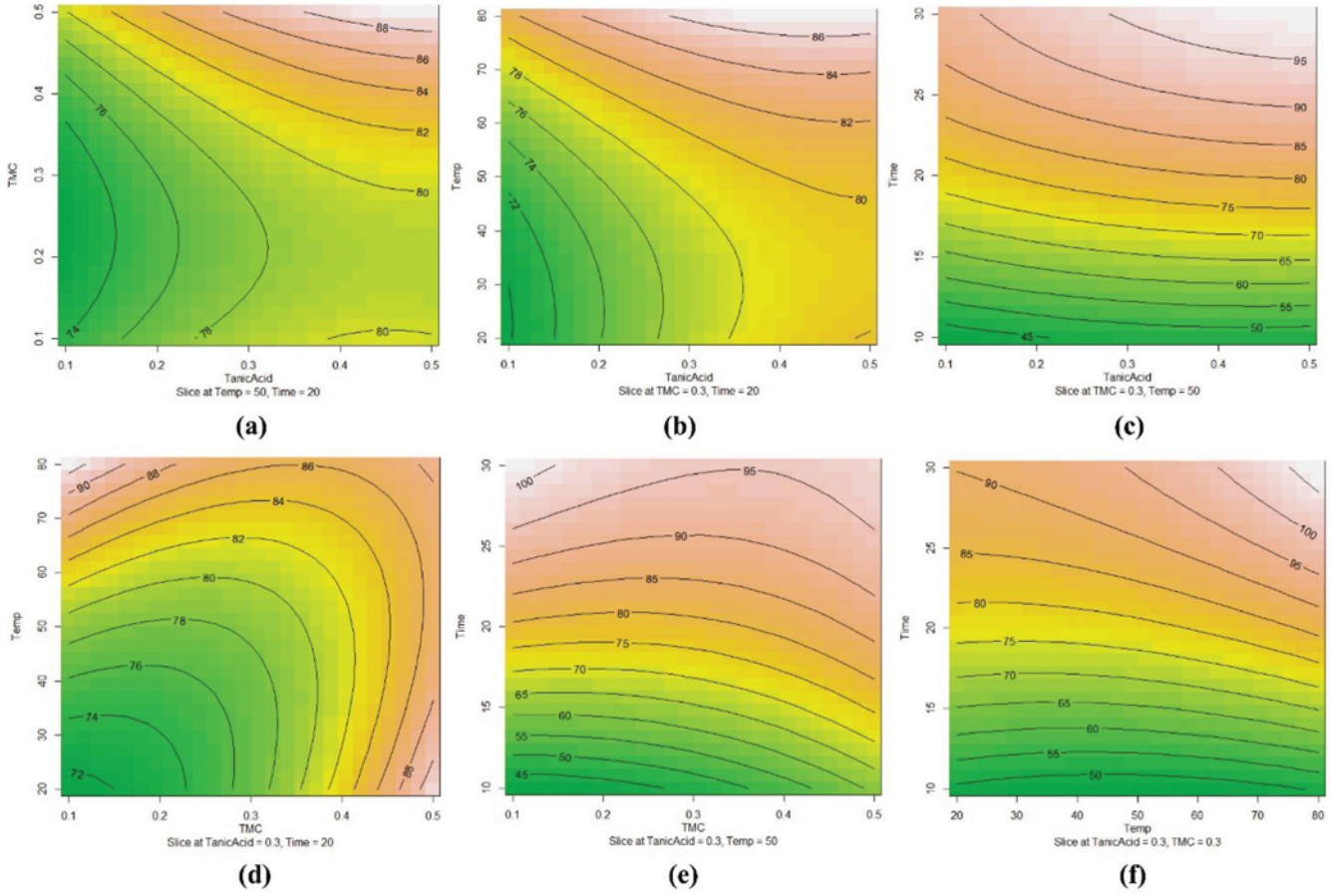

Fig. 4. Contour plots of DB71 removal efficiency as the function of independent variables: (a) TA and TMC (b) TA and temperature (c) TA and time (d) TMC and temperature (e) TMC and time and (f) temperature and time.

Table 6. Observed and predicted values of DB71 removal for the quadratic model

Run no.	X1	X2	X3	R (%)	Predicted (%)	Run no.	X1	X2	X3	R (%)	Predicted (%)
1	12.5	35	1	72.83	74.87	33	6.90	16.3	5	92.33	94.13
2	12.5	35	3	71.53	72.06	34	12.5	35	1	89.12	91.59
3	12.5	35	5	68.33	69.25	35	12.5	35	3	75.58	74.87
4	12.5	35	1	74.33	74.87	36	12.5	35	5	72.42	72.06
5	12.5	35	3	72.13	72.06	37	5	35	1	70.23	69.25
6	12.5	35	5	69.73	69.25	38	5	35	3	95.1	97.00
7	12.5	35	1	74.83	74.87	39	5	35	5	93.5	92.60
8	12.5	35	3	72.83	72.06	40	12.5	35	1	87.6	88.21
9	12.5	35	5	70.25	69.25	41	12.5	35	3	73.1	74.87
10	12.5	35	1	74.1	74.87	42	12.5	35	5	72.03	72.06
11	12.5	35	3	71.5	72.06	43	12.5	10	1	67.9	69.25
12	12.5	35	5	70.1	69.25	45	12.5	10	3	76.43	78.02
13	18.09	53.6	1	48.8	51.07	45	12.5	10	5	78.1	77.16
14	18.09	53.6	3	52.6	47.99	46	12.5	60	1	76.53	76.31
15	18.09	53.6	5	45.3	44.91	47	12.5	60	3	61.46	61.11
16	12.5	35	1	78.16	74.87	48	12.5	60	5	53.9	56.35
17	12.5	35	3	71.73	72.06	49	20	35	1	49.5	51.59
18	12.5	35	5	69.43	69.25	50	20	35	3	53.1	52.74
19	18.09	16.3	1	61.33	59.78	51	20	35	5	51.3	51.52
20	18.09	16.3	3	59.1	59.61	52	12.5	35	1	45.2	50.30
21	18.09	16.3	5	58.63	59.45	53	12.5	35	3	76.14	74.87
22	12.5	35	1	75.6	74.87	54	12.5	35	5	72.73	72.06
23	12.5	35	3	71.53	72.06	55	12.5	35	1	68.5	69.25
24	12.5	35	5	74.43	69.25	56	12.5	35	3	74.14	74.87
25	6.9	53.6	1	83.25	80.17	57	12.5	35	5	72.73	72.06
26	6.9	53.6	3	73.1	74.72	58	12.5	35	1	67.33	69.25
27	6.9	53.6	5	68.3	69.27	59	12.5	35	3	74.24	74.87
28	12.5	35	1	65.83	74.87	60	12.5	35	5	72.03	72.06
29	12.5	35	3	70.83	72.06	61	12.5	35	1	70.33	69.25
30	12.5	35	5	68.33	69.25	62	12.5	35	3	74.6	74.87
31	6.90	16.3	1	98.9	96.66	63	12.5	35	5	71.53	72.06
32	6.90	16.3	3	72.83	74.87						

of polymerization for composite membrane synthesis.

Optimization with the Solver "Add-ins" program on the Excel spreadsheet was done to achieve the optimal membrane performance. The criterion for optimization was optimum water flux and DB71 removal. In this stage, all parameters have simultaneously run for the predicted desirable criteria at the optimum performance. The predicted optimum operational conditions were: tannic acid concentration of 0.15 g/L; TMC concentration of 0.25 g/L, reaction time of 18.16 min and temperature of 69.20 °C, and the water flux was estimated to be 49.99 L/m^2·h. Also, additional laboratory experiments for evaluating the validity of the results predicted by the model showed that the experimental data were in good consistency with the predicted data through the regression model (the water flux at the laboratory experiments was 48.23±1.56). Therefore, according to the results of optimization, experimental design with RSM method and also optimization of the process through this method could be used as a good method for process efficiency assessment.

3. Permeation and DB71 Rejection Experiments

To evaluate the performance of composite membrane, the rejection data of DB71 were also studied using the RSM method. So, in this step, the main operational parameters such as the initial DB71 concentration, time and operating pressure were taken to specify the optimal operation conditions. The combined effects of initial DB71 concentration, time and applied pressure (bar) on the DB71 removal (Y) were determined by RSM. The experimental and predicted values for DB71 removal efficiency (%) by prepared composite membranes using quadratic model are presented in Table 6. According to the results, the predicted values were best in line with the experimental data (R^2>0.98), which indicated the quadratic model had a good agreement for predicting the data of DB71 removal.

The results of analysis of variance analysis (ANOVA) and regression analysis for quadratic model for DB71 removal are shown in Table 7. The model competency was investigated using the p-value, F-value, regression coefficient (R^2) and lack of fit [41]. Low P-value (<0.05), high F-value, high regression coefficient (R^2>0.98)

Table 7. Analysis of variance (ANOVA) and regression analysis for the quadratic model

Analysis of variance (ANOVA)					
Model formula in RSM (X1, X2, X3, X4)	DF	Sum of squares	Mean squares	F-value	Probability (P)
FO	3	6039.2	2013.07	3325.296	<0.0002
TWI	3	76.6	25.53	42.176	0.0003846
PQ	3	166.2	55.4	91.5146	<0.0002
Residuals	53	32.1	0.61	-	-
Lack of fit	17	12.5	0.74	1.3583	0.2145
Pure error	36	19.5	0.54	-	-
Regression analysis for the quadratic model					
Parameter		Coefficient estimate	Std. error	t Value	Pr(>|t|)
(Intercept)		72.24964	0.18588	388.6844	2.2×10^{-16}
X_1		−20.7533	0.24012	−86.4305	0.00187
X_2		−10.6333	0.24012	−44.2841	0.00025
X_3		−2.80167	0.12006	−23.336	2.2×10^{-16}
$X_1{*}X_2$		4.3889	0.59895	7.3276	1.34×10^{-9}
$X_1{*}X_3$		1.58	0.29408	5.3727	0.00125
$X_2{*}X_3$		−1.95	0.29408	−6.6309	0.000245
X_2^2		−5.23464	0.31933	−16.3927	2.2×10^{-16}
X_3^2		−0.48472	0.20795	−2.331	0.02359
Multiple R^2=0.978; Adjusted R^2=0.968; Predicted R^2: 0.953,Lack of fit: 0.214					

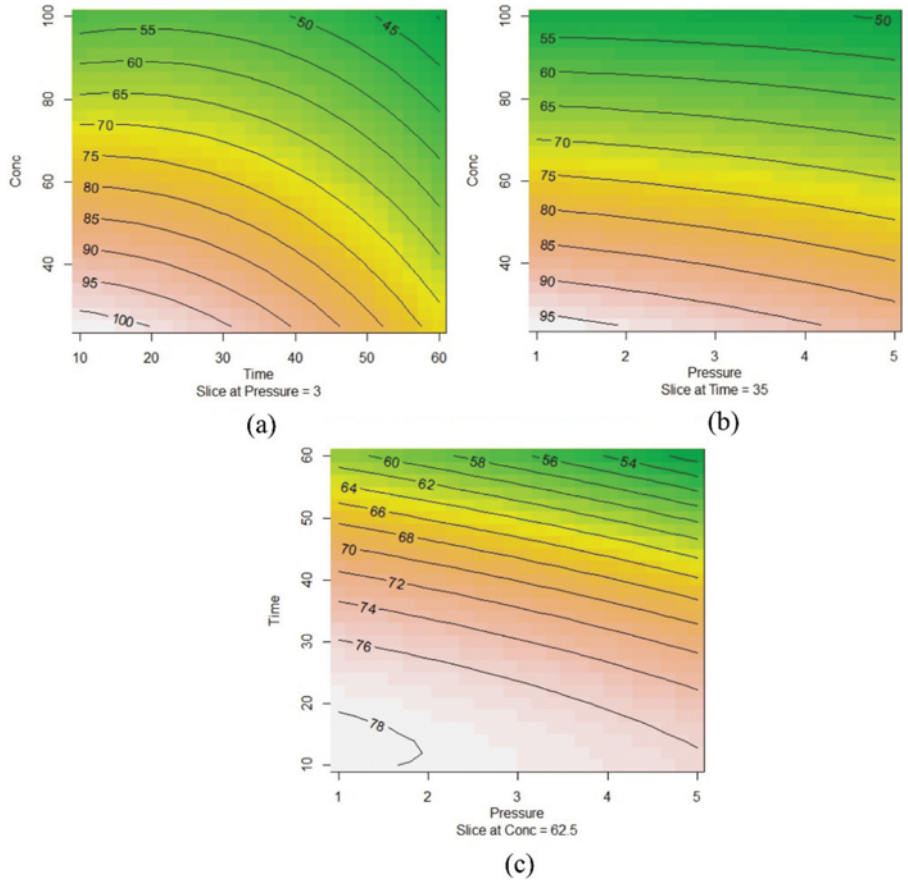

Fig. 5. Contour plots of DB71 removal efficiency as the function of independent variables: (a) Concentration of DB71 and time (b) Concentration of DB71 and Pressure and (c) time and pressure.

and insignificant lack of fit (0.21) showed that quadratic model had a good ability for analyzing the DB71 removal using nanocomposite membrane. Also, a high regression coefficient (R^2) value (close to one) and its good agreement with R^2_{adj} represented that there was a high correlation between the experimental and predicted values. In addition, the ANOVA results showed that the effect of all variables (X_1: initial DB71 concentration; X_2: time and X_3: applied pressure) was significant. The maximum t-value (20.75) for DB71 concentration showed that the DB71 concentration was the most effective parameter for DB71 removal (with reverse effect), while the applied pressure was the least effective parameter, and the interaction between X1, X2 and X3 was significant. In addition, contour plots of DB71 removal efficiency are shown in Fig. 5. Indeed, the operating pressure acts as a driving force for passing the DB71 through the membrane pores, and further, the presence of DB71 on the membrane surface could lead to decreasing the charge of the membrane surface; thus, the rejection of DB71 decreased with increasing operating pressure and initial dye concentration.

As mentioned, the RSM results were run on the Solver "Add-ins" in Excel spreadsheet to determine the optimization condition. The optimal criterion for this stage was the maximum removal efficiency for DB71. According to the optimization, the predicted optimum operational conditions were: initial DB71 concentration of 30.31 mg/L; time of 16.96 min, applied pressure of 1.16 bar, and the maximum removal efficiency was 98.46%. Also, the laboratory experiments were employed to determine the validity of the results predicted by the model. Based on the results, the removal efficiency of experimental data (98.46%) had good consistency with predicted data by the regression model.

4. Performance of Prepared Membrane at Optimum Condition

The results of the performance of membrane prepared at optimum conditions for removal of DB71, Reactive Blue 19 and methylene blue are shown in Fig. 6. According to the results, rejection of DB71 and Reactive Blue 19 was higher than methylene blue, and rejection (%) decreased with increasing in initial dye concentration because the mobility of methylene blue in the membrane pores was limited.

5. Antifouling Estimation of Composite Nanofiltration Membranes

Antifouling is an important parameter for application of the membrane [42]. The interactions between foulant and nanocomposite membrane such as hydrogen bonding, van der Waals attractions, hydrophobic interactions and electrostatic interactions play an important role in adsorption and/or rejection or permeation of the foulant. Minimization of the adsorption mechanism can help to reduce membrane fouling [43]. The antifouling assessment of the prepared nanocomposite membrane was carried out with mixed solution of organic (HA and BSA) and salt (Na_2SO_4). Antifouling examination was done over an operation time of 25 h. The results of antifouling evaluation are shown in Fig. 7.

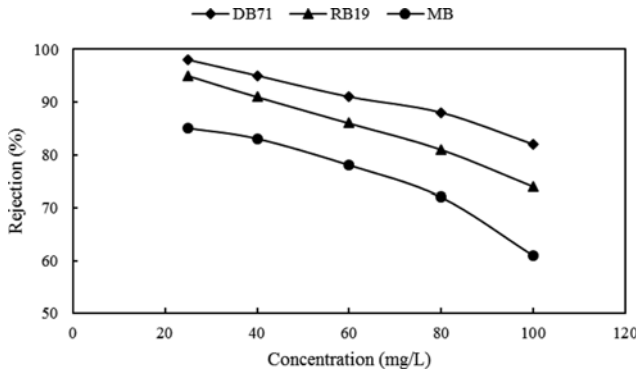

Fig. 6. Performace of prepared membrane at optimum condition for preparation of membrane and operational condition.

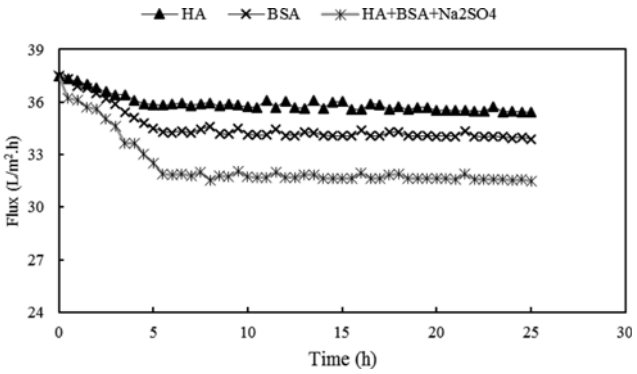

Fig. 7. Antifouling evaluation of nano-composite membrane in different time-fluxes ((HA: 0.1 g/L; BSA: 0.1 g/L; Na_2SO_4: 0.5 g/L; pH: 7±0.15, 1 bar).

According to the results, water flux precipitously fell off during the initial 7 h and then decreased slightly. Nanocomposite membrane during the initial operating time and applied pressure was more compacted, and decreasing the water flux during this time was sharp. In addition, the concentration polarization rate and the roughness of membrane surface play a special role in the fouling phenomenon. Phenolic functional groups on the membrane make a good cross-linking on the membrane and increase the hydrophilicity of the membrane surface, which improves the antifouling property [35]. The FDR values for prepared nanocomposite membrane were 5.57 and 9.62 and 16.11% for HA, BSA and mixed organic and salt pollutant (HA+BSA+Na_2SO_4), respectively. The higher FDR values refer to the worse antifouling properties and there are remarkable foulant deposition and adsorption. The FRR values were 89.9, 87.2 and 86.56% with deionized water cleaning and 91.48, 90.35 and 89.82% with ultrasound for HA, BSA and mixing organic and salt pollutant, respectively. Higher FRR values show that foulants have fragilely appended on the membrane surface and easily separated through the simple cleaning. Functional groups on the nanocomposite membrane are more likely the main reason for these properties of the membrane [35].

6. Fouling Study of Composite Nanofiltration Membrane

Water flux reduction, rising operational and maintenance costs, and loss to life-time of the membrane are the main negative effects of membrane fouling. Modification of the membrane top layer through the hydrophilic agents has been considered as a positive effect on the fouling resistance [43]. Electrostatic or hydrophobic interactions, hydrogen bonding and van der Waals attraction have been the main mechanism of fouling which can occur [44]. Hermia empirical model has been popularly employed to determine

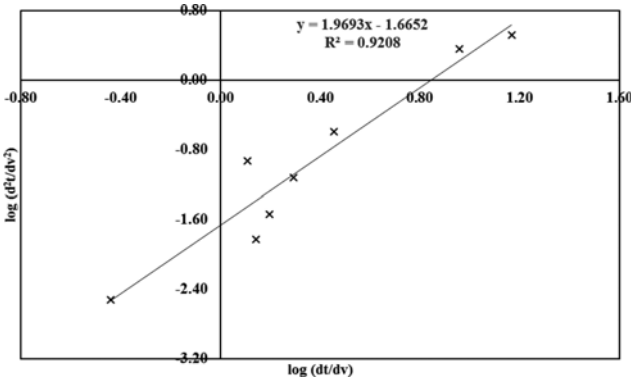

Fig. 8. Fouling analysis for HA filtration of nano composite membrane (DB71: 50±2.54 mg/L, pH: 7±0.15, 1 bar).

the mechanism of fouling. The equation of this model is as follows:

$$\frac{d^2t}{dv^2} = k\left(\frac{dt}{dv}\right)^n$$

where, v and t refer to volume (L) and time (s), k represents the coefficient of blocking law (units depends on n) and n (dimensionless) shows the blocking law filtration exponent. In this model, n values indicate different modes of fouling: cake filtration on top of the membrane (n=0), pore sealing with superposition (n=1), internal pore constriction (n=1.5) and pore sealing (n=2) [45]. A plot of the fouling mechanism using Hermia model is shown in Fig. 8. According to the result, n=1.97 indicated that pore sealing is the responsible mechanism for membrane fouling. Thus, it indicates that the pore sizes of nanocomposite membranes are larger than molecular sizes of the foulants and it could not penetrate into the pores and only resulted in surface fouling. Hydroxyl group on the nanocomposite membrane prepared hindered the contact between foulant and membrane surfaces. The results of Hermia modeling had good compatibility fouling study (experimental study); thus, it could be concluded that the Hermia model can be used for fouling mechanism and membrane recovery.

CONCLUSION

Nano-composite membrane synthesis by natural material (tannic acid) and acyl chloride (TMC) through interfacial polymerization was investigated. The main results of this study were as follow:

- The results of structural properties, DB71 rejection, fouling mechanism and antifouling properties showed that prepared membrane has good characteristics and could be valuable in the water industry.
- Nanocomposite membranes were more hydrophilic than support membrane.
- Interfacial polymerization can improve the removal efficiency of DB71.
- Increase in applied pressure incremented the pure water and solute permeability.
- According to the results, fouling mechanism is pore sealing (n=1.97).
- The potential application of the prepared nano-composite membranes can enhance in water treatment industry.

ACKNOWLEDGEMENT

This research was part of a Ph.D. dissertation and has been financially supported by a grant (Project No: 94-04-46-28520) from Center for Water Quality Research, Institute for Environmental Research, Tehran University of Medical Sciences, Tehran, Iran. The authors would like to thank the Department of Environmental Health Engineering, School of Public Health, Tehran University of Medical Sciences for their collaborations.

REFERENCES

1. E. Forgacs, T. Cserhati and G. Oros, *Environ. Int.*, **30**, 953 (2004).
2. D. Charumathi and N. Das, *Desalination*, **285**, 22 (2012).
3. A. Maleki, A. H. Mahvi, R. Ebrahimi and Y. Zandsalimi, *Korean J. Chem. Eng.*, **27**, 1805 (2010).
4. A. Mahvi, M. Ghanbarian, S. Nasseri and A. Khairi, *Desalination*, **239**, 309 (2009).
5. E. Bazrafshan, F. K. Mostafapour, A. R. Hosseini, A. Raksh Khorshid and A. H. Mahvi, *J. Chem.*, **2013**, 1 (2012).
6. M. Shirmardi, A. Mesdaghinia, A. H. Mahvi, S. Nasseri and R. Nabizadeh, *J. Chem.*, **9**, 2371 (2012).
7. G. Mezohegyi, F. P. Van der Zee, J. Font, A. Fortuny and A. Fabregat, *J. Environ. Manage.*, **102**, 148 (2012).
8. T. K. Sen, S. Afroze and H. M. Ang, *Water Air Soil Pollut.*, **218**, 499 (2011).
9. E. Basturk and M. Karatas, *J. Photochem. Photobiol., A*, **299**, 67 (2015).
10. S. S. Mirzadeh, S. M. Khezri, S. Rezaei, H. Forootanfar, A. H. Mahvi and M. A. Faramarzi, *IAEH*, **12**, 6 (2014).
11. A. M. Ferreira, J. A. Coutinho, A. M. Fernandes and M. G. Freire, *Sep. Purif. Technol.*, **128**, 58 (2014).
12. M. Ahmadian, N. Yosefi, A. Toolabi, N. Khanjani, S. Rahimi and A. Fatehizadeh, *Asian J. Chem.*, **24**, 3094 (2012).
13. A. Dalvand, E. Gholibegloo, M. R. Ganjali, N. Golchinpoor, M. Khazaei, H. Kamani, S. S. Hosseini and A. H. Mahvi, *Environ. Sci. Pollut. R.*, **23**, 16396 (2016).
14. S. Ashrafi, H. Kamani, H. Soheil Arezomand, N. Yousefi and A. Mahvi, *Desalin. Water Treat.*, **57**, 14051 (2016).
15. S. D. Ashrafi, S. Rezaei, H. Forootanfar, A. H. Mahvi and M. A. Faramarzi, *Int. Biodeterior. Biodegrad.*, **85**, 173 (2013).
16. S. Pourfadakari, N. Yousefi and A. H. Mahvi, *Chin. J. Chem. Eng.*, **24**, 1448 (2016).
17. F. Gholami-Borujeni, A. H. Mahvi, S. Nasseri, M. A. Faramarzi, R. Nabizadeh and M. Alimohammadi, *Appl. Biochem. Biotechnol.*, **165**, 1274 (2011).
18. J. Luo and Y. Wan, *J. Membr. Sci.*, **438**, 18 (2013).
19. N. Yousefi, A. Fatehizedeh, K. Ghadiri, N. Mirzaei, S. D. Ashrafi and A. H. Mahvi, *Desalin. Water Treat.*, **57**, 11782 (2016).
20. Y. Ma, Y. Su, Y. Li and Z. Jiang, *Korean J. Chem. Eng.*, **32**, 1902 (2015).
21. W. Choi, S. Jeon, S. J. Kwon, H. Park, Y. I. Park, S. E. Nam, P. S. Lee, J. S. Lee, J. Choi and S. Hong, *J. Membr. Sci.*, **527**, 121 (2017).
22. W. I. Son, J. M. Hong and B. S. Kim, *Korean J. Chem. Eng.*, **22**, 285

(2005).
23. P. G. Ingole and N. P. Ingole, *Korean J. Chem. Eng.*, **31**, 2109 (2014).
24. F. Jahangiri, S. A. Mousavi, F. Farhadi, V. Vatanpour, B. Sabzi and Z. Chenari, *Korean J. Chem. Eng.*, **33**, 1028 (2016).
25. S. J. Park, W. Choi, S. E. Nam, S. Hong, J. S. Lee and J. H. Lee, *J. Membr. Sci.*, **526**, 52 (2017).
26. J. Yi, *Korean J. Chem. Eng.*, **12**, 391 (1995).
27. Y. W. Kim, J. J. Kim and Y. H. Kim, *Korean J. Chem. Eng.*, **20**, 1158 (2003).
28. D. L. Shaffer, M. E. Tousley and M. Elimelech, *J. Membr. Sci.*, **525**, 249 (2017).
29. S. J. Oh and L. H. Kim, *Korean J. Chem. Eng.*, **12**, 340 (1995).
30. K. P. Lee, G. Bargeman, R. de Rooij, A. J. Kemperman and N. E. Benes, *J. Membr. Sci.*, **523**, 487 (2017).
31. M. Khazaei, S. Nasseri, M. R. Ganjali, M. Khoobi, R. Nabizadeh, A. H. Mahvi, S. Nazmara and E. Gholibegloo, *IAEH*, **14**, 2 (2016).
32. A. Dalvand, R. Nabizadeh, M. R. Ganjali, M. Khoobi, S. Nazmara and A. H. Mahvi, *J. Magn. Magn. Mater.*, **404**, 179 (2016).
33. R. Rezaee, S. Nasseri, A. Mahvi, R. Nabizadeh, S. Mousavi, A. Rashidi, A. Jafari and S. Nazmara, *IAEH*, **13**, 1 (2015).
34. Z. Wang, H. Yu, J. Xia, F. Zhang, F. Li, Y. Xia and Y. Li, *Desalination*, **299**, 50 (2012).
35. H. Wu, B. Tang and P. Wu, *J. Membr. Sci.*, **428**, 425 (2013).
36. Y. Zhao, X. Hu, B. Jiang and L. Li, *Desalination*, **336**, 64 (2014).
37. M. A. Zazouli, S. Nasseri and M. Ulbricht, *Desalination*, **250**, 688 (2010).
38. J. Yin and B. Deng, *J. Membr. Sci.*, **479**, 256 (2015).
39. V. Vatanpour, S. S. Madaeni, R. Moradian, S. Zinadini and B. Astinchap, *J. Membr. Sci.*, **375**, 284 (2011).
40. S. Xia and M. Ni, *J. Membr. Sci.*, **473**, 54 (2015).
41. Y. Xue, H. Hou and S. Zhu, *Chem. Eng. J.*, **147**, 272 (2009).
42. Y. L. Ji, Q. F. An, Q. Zhao, W. D. Sun, K. R. Lee, H. L. Chen and C. J. Gao, *J. Membr. Sci.*, **390**, 243 (2012).
43. H. Wu, B. Tang and P. Wu, *J. Membr. Sci.*, **428**, 301 (2013).
44. Y. N. Wang and C. Y. Tang, *J. Membr. Sci.*, **376**, 275 (2011).
45. J. C. Crittenden, R. R. Trussell, D. W. Hand, K. J. Howe and G. Tchobanoglous, *MWH's water treatment: principles and design*, Wiley, New Jersey (2012).